Submitted to Chemical Science, Feb/17/2022

Validating Experiments for the Reaction $H_2 + NH_2^-$ by Dynamical Calculations on an Accurate Full-Dimensional Potential Energy Surface

Kaisheng Song,[1] Hongwei Song,[2,*] and Jun Li[1,*]

[1] *School of Chemistry and Chemical Engineering & Chongqing Key Laboratory of Theoretical and Computational Chemistry, Chongqing University, Chongqing 401331, P.R. China*

[2] *State Key Laboratory of Magnetic Resonance and Atomic and Molecular Physics, Wuhan Institute of Physics and Mathematics, Innovation Academy for Precision Measurement Science and Technology, Chinese Academy of Sciences, Wuhan 430071, China*

*: *Corresponding authors, emails:* hwsong@wipm.ac.cn (HS) and jli15@cqu.edu.cn (JL).

Abstract

Ion-molecule reactions play key roles in the field of ion related chemistry. As a prototypical multi-channel ion-molecule reaction, the reaction $H_2 + NH_2^- \rightarrow NH_3 + H^-$ has been studied for decades. In this work, we develop a globally accurate potential energy surface (PES) for the title system based on hundreds of thousands of sampled points over a wide dynamically relevant region that covers long-range interacting configuration space. The permutational invariant polynomial-neural network (PIP-NN) method is used for fitting and the resulting total root mean squared error (RMSE) is extremely small, 0.026 kcal mol^{-1}. Extensive dynamical and kinetic calculations are carried out on this new PIP-NN PES by the quasi-classical trajectory (QCT) method. The calculated rate coefficients for H_2 / D_2 + NH_2^- agree well with the experimental results, which show an inverse temperature dependence from 50 to 300 K, consistent with the capture nature of this barrierless reaction. The significant kinetic isotope effect observed by experiment is well reproduced by the QCT computations as well. In addition, we report a unique phenomenon of significant reactivity suppression by exciting the rotational mode of H_2, supported by both QCT and quantum dynamics (QD) calculations. Further analysis uncovers that exciting the H_2 rotational mode would prevent the formation of the reactant complex and thus suppress reactivity.

1. Introduction

Ion-molecule reactions are of vital significance wherever ions are present, such as in organic chemistry, discharged plasma, combustion, the Earth's ionosphere, biological signal processing, liquid solutions, as well as the interstellar medium (ISM).[1-4] Owing to difficulties both in experiment and theory, related investigations on the ion-molecule reactions are scarce and their dynamics awaits to explore.[5] In this work, we will focus on the following ion-molecule reaction,

$$H_2 + NH_2^- \leftrightarrow H^- + NH_3, \quad \Delta H_{rxn}(0\ K) = -2.419\ kcal\ mol^{-1} \qquad (R1)^6$$

In R1, the neutral molecule H_2 reacts with the amino radical anion NH_2^- to yield NH_3 and H^- through a proton transfer. Only few relevant investigations, by theory or experiment, were reported.[1, 4, 7-11] Bohme *et al*. measured the rate coefficients of R1 independently in forward (k_f) and reverse (k_r) directions, and the equilibrium constant (K_{eq}) at 297 K in a flowing afterglow system. The corresponding rate coefficients were $k_f = (2.3\pm0.5)\times10^{-11}$ and $k_r = (9.2\pm1.8)\times10^{-13}$ $cm^3molecule^{-1}s^{-1}$, and the ratio of the rate coefficients was in good agreement with the equilibrium constant.[7] Using an ion trap equipment, Otto *et al.* obtained k_f in the temperature range from 300 to 8 K in order to reach conditions resembling the ISM environments.[1] At 300 K, their rate coefficient k_f was consistent with the earlier experiment, both of which were significantly below the capture-limited Langevin rate. As the temperature decreases, k_f increases until to a maximum at 20 K. From 20 to 8 K, k_f was found to decrease again.[1]

Theoretical studies[1, 4, 8-11] are useful to confirm the reaction profile of R1. As shown in **Figure 1**, pre- and post-reaction complex wells, $NH_2^-\cdots H_2$ (RC) and $H^-\cdots NH_3$ (PC), can be formed along the reaction path. There are two submerged barriers, TS1 and TS2, along the R1 reaction. A significantly high barrier, TS3, leads to NH_4^-. Ample scrutinizes have been carried out to reveal the structures, ro-vibrational spectrum, and the ionization energies of the complexes, PC and NH_4^-, and their photoelectron spectrum.[8, 10, 12-27] These investigations concluded that the PC ion is more stable due to the ion-dipole attraction, as it can be described as a hydride ion solvated by an ammonia molecule. The other form NH_4^- is a double-Rydberg molecular anion of T_d geometry.[21] There was a

relatively high barrier, TS3, that separates PC and NH_4^-,[9] resulting in a long-lived NH_4^-. Indeed, both PC and NH_4^- were experimentally identified in their photoelectron spectra,[23-25, 27] thanks to their different features, as they probe different regions[27] of the neutral NH_4 potential energy surface (PES).[28]

For the forward reaction of R1, which is barrierless and exothermic, the rate coefficients are more than a factor of ten below the capture limit, an indication of heavy dynamical effect during the reaction. The temperature dependence of k_f, particularly at low temperatures between 100 and 300 K, has been partly rationalized by the combination of the statistical model and the steric hindrance of the RC complex well.[1] At temperatures below 100 K, the discrete quantum mechanical nature of the system was suggested to be taken into account,[1] which, however, are still challenging for penta-atomic reactions.[29] By introducing an adjusted temperature dependent term, Gianturco *et al.* employed the variational transition state (VTST) approach to obtain temperature-dependent rate coefficients of R1 that are consistent with experiment over 300 ~ 8 K.[4] The statistical model may be invalid as the dynamic effect plays an important role.[30] For either quasi-classical trajectory (QCT) or quantum dynamical (QD) calculations, a reliable full-dimensional potential energy surface (PES) is required.[31] Thanks to advances in various neural network (NN)-based fitting methods,[32-35] reliable full-dimensional PESs for reactive systems with up to seven atoms[36-48] are reported by fitting hundreds of thousands of configurations, whose energies were determined at the explicitly correlated CCSD(T) with the AVTZ basis set (CCSD(T)-F12a/AVTZ).[49, 50] However, due to the long-range interactions between the negatively charged ions and the neutral molecules,[2] the PES of R1 covers a huge configuration space, particularly in the reactant or product channels, making the construction of the full-dimensional accurate PES more challenging. Recently, Pan *et al.* reported a full-dimensional PES for the title reaction based on about 46 000 points calculated at the level of CCSD(T)-F12a/AVTZ.[11] The fundamental invariants neural network (FI-NN) method[33] was used for fitting and the resulting PES is denoted as FI-NN PES hereafter.[11] The rate coefficients on the FI-NN PES were slightly higher than the experiment.[11] The FI-NN PES did not include the NH_4^-

channel and the description of the long-range part was not sufficiently accurate. Further, in order to provide reliable estimation for the vertical detachment energy (VDE) of the PC and NH_4^- anions, additional diffuse basis functions were suggested to be included,[26] but were not included in the FI-NN PES. Indeed, in our previous photodetachment simulations, a local PES around the PC and NH_4^- anions was developed based on about 28 000 points computed at the level of UCCSD(T) with the default basis set AVTZ and an additional diffuse basis set for the N atom, denoted as UCCSD(T)/AVTZ′ hereafter.[27] As demonstrated in our previous work,[27] the results calculated at the CCSD(T)/AVTZ′ level were consistent with available experiment and theoretical data, including the VDE, the geometries, the photoelectron spectra, *etc*.

In this work, 98 154 points sampled in a large dynamically related configuration space were calculated at the UCCSD(T)/AVTZ′ level and fitted by the PIP-NN approach. Then QCT computations are carried out to study the kinetics and dynamics of the $H_2 + NH_2^-$ reaction. Our calculations reveal a novel mode specificity: the excitation of the H_2 rotational motion significantly suppresses the reactivity of the title ion-molecule reaction. To provide solid support on the dynamical findings, QD simulations are performed on the same PES as well. The remaining of the work is organized as follows. **Section 2** details the *ab initio* calculation, followed by the description of the PIP-NN PES in **Section 3**. The kinetics and dynamical results are given in **Section 4** and **5**, respectively. Finally, a summary of conclusions is given in **Section 6**.

2. Ab initio calculations

All electronic structure calculations were done by the MOLPRO program package.[51] The geometries of the stationary points were firstly optimized at the level of UCCSD(T)/AVTZ′ and are shown in **Figure S1**. The harmonic frequencies and energies were then computed at the same level. Additional computations were carried out at the levels of CCSD(T)/AVTZ′ and CCSD(T)-F12a/AVTZ for comparison.

As shown in **Figure 1**, NH_2^- and H_2 first form the RC complex, which is -4.24 kcal mol^{-1} relative to the asymptotic reactant energy. The RC complex is of C_{2v} symmetry within a plane. The

internuclear distance H_2N^-—H_2 is 2.194 Å at the level of UCCSD(T)/AVTZ′. The H—H distance of the H_2 moiety is slightly enlarged from 0.743 to 0.765 Å, as shown in **Figure S1**. The geometry of the NH_2 moiety is nearly unchanged from the reactant to the RC complex. TS1, a planar geometry as well, is only 2.85 kcal mol^{-1} higher than that of RC, and 1.39 kcal mol^{-1} lower than that of the reactants, at which the distances of the forming N—H bond and the broken H—H bond are 1.510 and 0.919 Å, respectively. The PC complex well is 14.57 kcal mol^{-1} lower than the reactant energy. PC is stable since the interaction is mainly dominated by the ion-dipole interaction. RC is mainly stabilized by the ion-quadrupole interaction, as H_2 has no dipole. Therefore, this PC complex is well stabilized and thus can be detected experimentally. PC can isomerize to itself via TS2 and then dissociate to the products $NH_3 + H^-$. The dissociation energy is 8.78 kcal mol^{-1}. The product energy is -5.79 kcal mol^{-1} relative to the reactant energy, namely, R1 is exothermic. PC can isomerize to another complex NH_4^- of T_d symmetry via TS3, which is 29.77 and 17.51 kcal mol^{-1} higher than PC and NH_4^-, respectively.

As shown in **Figure S1**, the UCCSD(T)/AVTZ′ and CCSD(T)/AVTZ′ calculations give nearly identical geometries, which, however, differ slightly from those calculated at the CCSD(T)-F12a/AVTZ level. The deviation for the N—H bond distance is as large as 0.026 Å at RC and 0.018 Å at TS3, respectively. **Table S1** compares the harmonic frequencies among different levels. Again, they agree well with each other.

Note that the CCSD(T)-F12a/AVTZ energies are significantly different from the UCCSD(T)/AVTZ′ ones. As shown in **Figure 1**, the differences are -0.20, -0.47, -0.43, -0.45, -0.46 kcal mol^{-1} for RC, TS1, PC, TS2, and the products, respectively. For TS3 and NH_4^-, the deviations are 2.93 and 1.91 kcal mol^{-1}, respectively. **Table 1** summarizes the zero-point vibrational energy (ZPE) corrected energies of the stationary points at different levels. One can see that the results are sensitive to the calculation levels. The largest discrepancy between CCSD(T)-F12a/AVTZ and UCCSD(T)/AVTZ′ exists for TS3, 2.64 kcal mol^{-1}. The ZPE corrected reaction energy of the

separated products is -2.18 kcal mol^{-1} at the UCCSD(T)/AVTZ′ level, comparable to the ATcT value -2.42 kcal mol^{-1}.[6]

3. PIP-NN PES

As has been detailed in our previous work,[36-45] developing PESs consists of three procedures: sampling configurations in dynamical relevant regions, calculating their energies, and fitting them. For ion-molecule reactions, long-range interaction plays a key role in their dynamics and kinetics.[2] Therefore, the sampling should cover sufficient large configuration space to provide adequate description of all dynamically relevant regions. Previously, about 23 200 points were sampled to cover the regions around PC and NH_4^-.[27] In this work, 14 810 initial points were first sampled by varying the distances and orientations between H_2 and NH_2^-, and between H^- and NH_3. The center-of-mass (COM) distances between reactants or between products were up to 50 Å but with sparse grids, as the interaction along the COM distance (R_{COM}) is mainly determined by the electrostatic interaction.[2] Denser grids were used for intramolecular coordinates in asymptotic reactant and product channels, the vicinities around the stationary points and the minimum energy paths (MEPs). Then, a primitive PES was obtained.

Based on this preliminary PES, QCT calculations with specific vibrational/rotational/translational temperatures, up to 1500 K, were carried out. All dynamically relevant regions can be explored to verify the performance of the PES, which may be unreliable for regions lacking points. Thus, data points in these regions can be sampled and used to patch up the PES. The procedure was repeated to improve the PES until all relevant dynamical results were converged. To eliminate points that are too close to the existing data set, the generalized Euclidean distance was used. In the present work, the criterion is the generalized Euclidean distance $\chi\left(\{r_i\}\right)=\sqrt{\sum_i^{10}\left|\vec{r}_i-\vec{r}_i'\right|^2}<0.1-1.0$ Å defined in terms of the internuclear distances between two points, $\{\vec{r}_i\}$ and $\left\{\vec{r}_i'\right\}$, in the data set. All permutationally equivalent points among the four hydrogen atoms (4! = 24) were considered in such screenings. Key properties of the system,

including geometries, frequencies, and energies of the stationary points, regions around the minimum energy paths (MEPs), and dynamical outcome were tested to confirm the quality and convergence of the PES.

A total of 98 154 points were sampled and calculated at the level of UCCSD(T)/AVTZ′. As shown in **Figure 2**, these points were sampled in a very large configuration space: the H_2N—H_2 and H_2NH—H distances are as long as 50 Å, which are necessary for well describing the long-range interactions. Indeed, both long- and short-range regions are well covered to guarantee the quality of the resulting PES. These points were fitted by the permutation invariant polynomial - neural network (PIP-NN) approach.[52, 53] Please refer to the **Supporting Information** (**SI**) for more details. Briefly, the input layer of the NN contains 207 PIPs. The two hidden layers were chosen to be consisted of 15 and 80 neurons, respectively, yielding 4481 fitting parameters. The overall root mean squared error (RMSE) of the final PES is only 0.026 kcal mol^{-1}, and the RMSEs for the training/validation/test sets are 0.025/0.030/0.032 kcal mol^{-1}, respectively. The inset plot of **Figure 2 (a)** represents the fitting errors versus the *ab initio* energies. Clearly, the small fitting errors are evenly distributed within a large energy range from -16 to 100 kcal mol^{-1}. Most of these points have small fitting errors. As shown in **Figure S2**, the percentage of the energy points with the unsigned error less than 0.030 kcal mol^{-1} is 85.4%.

The energies, structures, and harmonic frequencies of the stationary points on the current PES are shown in **Figure 1, S1,** and **Table S1**, respectively. One can see that the PIP-NN PES reproduces well the target UCCSD(T)/AVTZ′ results. The deviations for energies, geometries (bond lengths and angles), and harmonic frequencies are within 0.02 kcal mol^{-1}, 0.005 Å, 0.2°, and 36.8 cm^{-1}, respectively.

The inset plot of **Figure 2(b)** plots the contour of the PES along the broken bond r_{HH} (H_2NH—H) and the forming bond r_{NH} (H_2N—H_2), up to 8 Å. All other coordinates were fixed at TS1. The energy is taken from -15 to 60 kcal mol^{-1} with an interval of 5 kcal mol^{-1}. The two complexes RC and PC, and TS1 are clearly shown.

The potential energies of the PES along the MEPs through TS1, TS2 and TS3 are displayed in **Figure 3 (a)**, **(b)** and **Figure S3**, respectively. Clearly, the direct *ab initio* calculations are in excellent agreement with the PIP-NN PES. As mentioned above, it is challenging to reasonably describe the long-range interaction between ion and neutral molecule. As shown in **Figure 3 (c)** and **(d)**, in both reactant and product channels, the interaction potentials of the PIP-NN PES are in excellent agreement with the direct *ab initio* calculations. The deviations between the PES and the *ab initio* calculations are within 0.02 – 0.04 kcal mol^{-1} even if the distances reach 50 Å, where the interaction energy from the *ab initio* calculations is still not converged. Overall, both long- and short-range regions are well represented by the current PES with high accuracy.

4. Kinetics

At each temperature of 50, 100, 150, 200 and 300 K, 2 ~ 25 $\times 10^4$ trajectories were carried out by the QCT approach (See **SI** for calculation details) and the corresponding statistical errors are all less than 5%. The reactivity to form NH_4^- is negligible due to the significantly higher barrier height of TS3 and not discussed further.

Figure 4 (a) displays the QCT rate coefficients on the PIP-NN PES as a function of temperature. Available theoretical and experimental results[1, 4, 7, 11] are also shown for comparison. The experimental results measured by Otto *et al.* showed a negative dependence between 20 to 300 K and a positive dependence from 8 to 20 K.[1, 11] Similarly, QCT calculated thermal rate coefficients on this new PIP-NN PES show the inverse temperature dependence from 50 to 300 K. However, they are higher than experiment. In order to partly remedy the ZPE leakage issue in the QCT,[54] the hard ZPE constraint method was employed. Namely, only those reactive trajectories with the vibrational energy of the product NH_3 larger than or equal to its ZPE (21.52 kcal mol^{-1}) were considered in the statistics. The corresponding results are marked as "hard-ZPE". As shown in **Figure 4 (a)**, "hard-ZPE" QCT results on the PIP-NN PES are in line with those QCT data on the FI-NN PES,[11] and the ratios of them to the measurements are about 1.52 ~ 2.82. Gianturco *et al.* employed the variational transition-state theory (VTST) to determine the rate coefficients of R1 at 8

~ 300 K. The calculated results were in good agreement with experiment by introducing a temperature-dependent scaling term.[4]

Isotope effect could provide further insight into the dynamics. Otto *et al.* measured the rate coefficients for the $D_2 + NH_2^- \rightarrow D^- + NH_2D$ reaction.[1] The trend of the measured rate coefficients is similar to that of R1. Starting from 8 K, the rate coefficient increases sharply and reaches the maximum at 20 K, and then goes down gradually as the temperature further increases. The QCT computations were also carried out at 50 ~ 300 K. As shown in **Figure 4 (b)**, the calculated results are consistent with the measured results but apparently higher. With the hard ZPE constraint, the agreement is improved. The overestimation of the QCT results may be caused by the incapability in describing quantum effects such as tunneling and ZPE. **Figure 4 (c)** shows the kinetic isotope effect (KIE) for the $H_2/D_2 + NH_2^-$ reaction, which is defined as k_{H2}/k_{D2}. Clearly, one can see that with the hard-ZPE constraint, the QCT KIEs agree well with the experiment: at 100 and 300 K. The experimental KIEs are 1.929 and 2.594, comparable to the theoretical values of 2.134 and 2.486, respectively. Both experiment and theory indicate that reactivity is significantly suppressed by substituting H_2 by D_2.

5. **Dynamics**

In the experiment by Otto *et al.*, the reactants NH_2^- and H_2 were prepared exclusively at the ground electronic and vibrational states. The ratio between the ortho and para rotational state of H_2 was 3:1.[1] Therefore, it is interesting to investigate the role of the ortho and para components of H_2 on the reactivity. To this end, we carried out QCT computations for H_2 (j=0, 1, 2) + $NH_2^- \rightarrow H^- + NH_3$.

1 ~ 70 $\times 10^4$ trajectories were carried out at the collision energies (E_c) of 1.0, 2.0, 5.0, 8.0, 10.0, 15.0, 20.0 kcal mol^{-1}, respectively. The corresponding statistical errors are all less than 5%. **Figure 5 (a)** shows the calculated ICSs for H_2 (j=0, 1, 2) + $NH_2^- \rightarrow NH_3 + H^-$ reaction as a function of E_c. One can see that, the ICS (j=0) drops rapidly at low E_c and then becomes almost flat at $E_c \geqslant 5$ kcal mol^{-1}, which is general in barrierless ion-molecule reactions.[55-58] In contrast, ICSs of j=1 are

dramatically lower than those of j=0, particularly at low E_c. For H_2 (j=2), the ICSs are even lower. Furthermore, the ICSs from j = 1 and 2 increase with the collision energy. This novel suppression of the rotational excitation of H_2 on the reactivity is in contrast to previous findings in the ion-molecule reactions $H_2 + OH^+$ and $H_2 + H_2O^+$,[59, 60] both with submerged barriers.

As QCT can't take the quantum effects into account, initial state-selected time-dependent QD computations were carried out for the reactions H_2 (j=0, 1) + $NH_2^- \rightarrow NH_3 + H^-$ (the QD calculation cost is too expensive for j = 2). The details for the QD method are given in **SI**. As depicted in **Figure 5 (a)**, the QD j = 0 ICSs are significantly lower than those from j = 1, consistent with the QCT calculations. However, the QD ICSs from j = 0 are significantly lower than the QCT ones, particularly at low E_c. For j = 1, QD and QCT results are consistent with each other. **Figure 5 (b)** shows the K-specific QD ICSs from j = 1 (K is the projection of the total angular momentum on the body-fixed z axis). Since the reactant NH_2 is launched from the ground rotational state, *i.e.* j_{23}=0, K=1 means that the reactant H_2 approaches NH_2 mainly in a direction perpendicular to the coordinate R (the straight line connecting the centroids of H_2 and NH_2). In contrast, H_2 prefers to approach NH_2 in a direction along R for K=0 (see also discussions below). Clearly, the ICS of K=0 is much larger than that of K=1. Note that the K=1 component has a weight of two in the statistics.

The long-range interaction usually plays an important role in determining the reactivity of a barrierless reaction.[61] **Figure 6** displays several one-dimensional cuts for the interactions between NH_2^- and H_2 (both fixed at their equilibriums) but at different orientations. Both the PIP-NN PES and the *ab initio* calculations show that there exists a significant stereodynamics effect: only the g and h orientations are attractive, and other orientations lead to repulsive interactions. The comparison shows that h is the most attractive orientation, leading to the RC well. The g orientation is less attractive at long distances and the interaction becomes repulsive at short distances. This is consistent with the different K-component contributions to the total ICSs from j = 1, as shown in **Figure 5(b)** and discussed above. Indeed, as shown in **Figure S4,** the interaction is apparently different when H_2 and NH_2^- approach each other at different orientations. Such special interaction is

significantly different from that in another ion-molecule reaction H_2 + H_2O^+,[62] in which most orientations result in attractive interactions.

To demonstrate the microscopic mechanism, the DCSs for the H_2(j = 0, 1, 2) + NH_2^- reaction at E_c = 1.0, 2.0, 5.0, 8.0, 10.0, 15.0, 20.0 kcal mol^{-1}, respectively, are plotted in **Figure 7**. For H_2 (j=0), the DCS shows an approximate forward-backward symmetric distribution at low E_c, which is caused by the relatively long-lived intermediate. With the increasing collision energy, the contributions from the forward and sideway scatterings become larger, as the direct striping and rebound mechanism becomes more and more important, which are supported by the correlations between impact parameter and the scattering angle shown in **Figure S6-S7**. For H_2 (j=1) and H_2 (j=2), the sideway and backward scatterings increase remarkably, particularly at low E_c. Furthermore, as shown in **Figure 8**, the distributions of the b-weighted impact parameter indicate that not only b_{max} but also the peak of the distributions for H_2 at j=1 and j=2 are apparently smaller than those for H_2 at j=0, again consistent with the microscopic mechanisms discussed above.

6. Conclusions

In this work, we report the globally accurate full-dimensional potential energy surface for the H_2 + NH_2^- system, which is fitted by using the permutation invariant polynomial – neural network method. The fitting error is only 0.026 kcal mol^{-1}. Due to the significant long-range interactions between H_2 and NH_2^- and between H^- and NH_3, a total of 98 154 points are sampled and calculated at the level of UCCSD(T)/AVTZ'. Not only regions for the abstraction channel and regions that involve NH_4^-, but also the long-range regions in the entrance and exit channels, are well described. The energy, geometry and harmonic frequencies of each stationary point, as well as the minimum energy path and some one-dimensional cuts are in excellent agreement with the *ab initio* results.

The quasi-classical trajectory (QCT) approach are then employed to calculate the rate coefficients of the H_2/D_2 + NH_2^- reaction within 50 ~ 300 K. Both theory and experiment show an inverse temperature dependence. QCT predictions are slightly higher than the experimental results.

The significant kinetic isotope effect observed by the experiment is well reproduced by theoretical calculations.

Impressively, both QCT and QD calculations found that exciting the rotational mode of H_2 significantly suppresses the reactivity. This unique feature can be attributed to the significant stereodynamical effect in the entrance channel. When the rotationally excited H_2 approaches NH_2^-, most orientations result in repulsive interactions that prevent the occurrence of reactions. This new suppression of reactivity of the ion-molecule reactions with a submerged barrier by exciting the reactant rotational mode enriches our understanding on the microscopic dynamics in various reactions.

Conflicts of interest

There are no conflicts to declare.

Acknowledgments

This work was financially supported by the National Natural Science Foundation of China (contract nos. 21973009 and 21973109), the Chongqing Municipal Natural Science Foundation (grant no. cstc2019jcyj-msxmX0087), the Venture and Innovation Support Program for Chongqing Overseas Returnees (grant no. cx2021071).

References:

1. R. Otto, J. Mikosch, S. Trippel, M. Weidemüller and R. Wester, *Physical Review Letters*, 2008, **101**, 063201.
2. J. Mikosch, M. Weidemüller and R. Wester, *Int. Rev. Phys. Chem.*, 2010, **29**, 589-617.
3. T. J. Millar, C. Walsh and T. A. Field, *Chem. Rev.*, 2017, **117**, 1765-1795.
4. F. A. Gianturco, E. Yurtsever, M. Satta and R. Wester, *J. Phys. Chem. A*, 2019, **123**, 9905-9918.
5. L. Li, B. Fu, X. Yang and D. H. Zhang, *Phys. Chem. Chem. Phys.*, 2020, **22**, 8203-8211.
6. B. Ruscic and D. H. Bross, Active Thermochemical Tables (ATcT) values based on ver. 1.122r of the Thermochemical Network (2021), available at ATcT.anl.gov, 2021).
7. D. K. Bohme, R. S. Hemsworth and H. W. Rundle, 1973, **59**, 77-81.
8. J. Kalcher, P. Rosmus and M. Quack, *Canadian Journal of Physics*, 1984, **62**, 1323-1327.
9. H. Cardy, C. Larrieu and A. Dargelos, *Chem. Phys. Lett.*, 1986, **131**, 507-512.
10. N. Matsunaga and M. S. Gordon, *J. Phys. Chem.*, 1995, **99**, 12773-12780.
11. M. Pan, H. Xiang, Y. Li and H. Song, *Phys. Chem. Chem. Phys.*, 2021, **23**, 17848-17855.

12. J. C. Kleingeld, S. Ingemann, J. E. Jalonen and N. M. M. Nibbering, *J. Am. Chem. Soc.*, 1983, **105**, 2474-2475.
13. D. Cremer and E. Kraka, *J. Phys. Chem.*, 1986, **90**, 33-40.
14. J. V. Ortiz, *J. Chem. Phys.*, 1987, **87**, 3557-3562.
15. M. Gutowski, J. Simons, R. Hernandez and H. L. Taylor, *J. Phys. Chem.*, 1988, **92**, 6179-6182.
16. J. V. Ortiz, *J. Phys. Chem.*, 1990, **94**, 4762-4763.
17. M. Gutowski and J. Simons, 1990, **93**, 3874-3880.
18. G. C. M. van der Sanden, E.-A. Reinsch, A. van der Avoird, P. E. S. Wormer and P. Rosmus, *J. Chem. Phys.*, 1995, **103**, 4012-4025.
19. S. Roszak, 1996, **105**, 7569-7572.
20. J. Melin and J. V. Ortiz, *J. Chem. Phys.*, 2007, **127**, 014307.
21. J. Simons and M. Gutowski, *Chem. Rev.*, 1991, **91**, 669-677.
22. J. Simons, *J. Phys. Chem. A*, 2008, **112**, 6401-6511.
23. J. V. Coe, J. T. Snodgrass, C. B. Freidhoff, K. M. McHugh and K. H. Bowen, *J. Chem. Phys.*, 1985, **83**, 3169-3170.
24. J. T. Snodgrass, J. V. Coe, C. B. Friedhoff, K. M. McHugh and K. H. Bowen, *Faraday Disc. Chem. Soc.*, 1988, **86**, 241-256.
25. S.-J. Xu, J. M. Nilles, J. H. Hendricks, S. A. Lyapustina and K. H. Bowen, *J. Chem. Phys.*, 2002, **117**, 5742-5747.
26. J. V. Ortiz, 2002, **117**, 5748-5756.
27. Q. Hu, H. Song, C. J. Johnson, J. Li, H. Guo and R. E. Continetti, *J. Chem. Phys.*, 2016, **144**, 244311.
28. J. Li and H. Guo, *Phys. Chem. Chem. Phys.*, 2014, **16**, 6753-6763.
29. J. Huang, J. Chen, S. Liu and D. H. Zhang, *J. Phys. Chem. Lett.*, 2020, **11**, 8560-8564.
30. L. Sun, K. Song and W. L. Hase, *Science*, 2002, **296**, 875-878.
31. J. Li, B. Zhao, D. Xie and H. Guo, *J. Phys. Chem. Lett.*, 2020, **11**, 8844-8860.
32. B. Jiang, J. Li and H. Guo, *J. Phys. Chem. Lett.*, 2020, **11**, 5120-5131.
33. R. Chen, K. Shao, B. Fu and D. H. Zhang, *J. Chem. Phys.*, 2020, **152**, 204307.
34. J. Li, K. Song and J. Behler, *Phys. Chem. Chem. Phys.*, 2019, **21**, 9672-9682.
35. J. Behler, *Chem. Rev.*, 2021, DOI: 10.1021/acs.chemrev.0c00868.
36. J. Qin and J. Li, *Phys. Chem. Chem. Phys.*, 2021, DOI: 10.1039/D0CP05206J.
37. Y. Liu, M. Bai, H. Song, D. Xie and J. Li, *Phys. Chem. Chem. Phys.*, 2019, **21**, 12667-12675.
38. M. Bai, D. Lu and J. Li, *Phys. Chem. Chem. Phys.*, 2017, **19**, 17718-17725.
39. J. Li, J. Chen, Z. Zhao, D. Xie, D. H. Zhang and H. Guo, *J. Chem. Phys.*, 2015, **142**, 204302.
40. Y. Liu and J. Li, *Phys. Chem. Chem. Phys.*, 2020, **22**, 344-353.
41. J. Li and H. Guo, *J. Chem. Phys.*, 2015, **143**, 221103.
42. M. L. Weichman, J. A. DeVine, M. C. Babin, J. Li, L. Guo, J. Ma, H. Guo and D. M. Neumark, *Nat Chem*, 2017, **9**, 950-955.
43. D. Lu, J. Li and H. Guo, *CCS Chem.*, 2020, **2**, 882–894.
44. D. Lu, J. Behler and J. Li, *J. Phys. Chem. A*, 2020, **124**, 5737-5745.
45. Y. Liu and J. Li, *ACS Omega*, 2020, **5**, 23343-23350.
46. L. Ping, Y. Zhu, A. Li, H. Song, Y. Li and M. Yang, *Phys. Chem. Chem. Phys.*, 2018, **20**, 26315-26324.
47. L. Tian, Y. Zhu, H. Song and M. Yang, *Phys. Chem. Chem. Phys.*, 2019, **21**, 11385-11394.
48. Y. Zhu, L. Tian, H. Song and M. Yang, *J. Chem. Phys.*, 2019, **151**, 054311.
49. T. B. Adler, G. Knizia and H.-J. Werner, *J. Chem. Phys.*, 2007, **127**, 221106.
50. L. Kong, F. A. Bischoff and E. F. Valeev, *Chem. Rev.*, 2011, **112**, 75-107.
51. W. H.-J. K. P. J. K. G. M. F. R. S. M. C. P. G. W. K. D. K. T.;, *Journal*, 2015.
52. B. Jiang and H. Guo, *J. Chem. Phys.*, 2013, **139**, 054112.
53. J. Li, B. Jiang and H. Guo, *J. Chem. Phys.*, 2013, **139**, 204103.
54. K. L. K. Lee, M. S. Quinn, S. J. Kolmann, S. H. Kable and M. J. T. Jordan, *J. Chem. Phys.*, 2018, **148**, 194113.
55. N. Bulut, J. F. Castillo, P. G. Jambrina, J. Kłos, O. Roncero, F. J. Aoiz and L. Bañares, *J. Phys. Chem. A*, 2015, **119**, 11951-11962.
56. Y. Paukku, K. R. Yang, Z. Varga, G. Song, J. D. Bender and D. G. Truhlar, *J. Chem. Phys.*, 2017, **147**, 034301.

57. Q. Yao, C. Xie and H. Guo, *J. Phys. Chem. A*, 2019, **123**, 5347-5355.
58. R. Wester, *Mass Spectrom Rev.*, 2021, DOI: https://doi.org/10.1002/mas.21705, 1-18.
59. H. Song, A. Li and H. Guo, *J. Phys. Chem. A*, 2016, **120**, 4742-4748.
60. H. Song, A. Li, H. Guo, Y. Xu, B. Xiong, Y.-C. Chang and C. Y. Ng, *Phys. Chem. Chem. Phys.*, 2016, **18**, 22509-22515.
61. H. Pan, F. Wang and K. Liu, *J. Phys. Chem. A*, 2020, **124**, 6573-6584.
62. A. Li, Y. Li, H. Guo, K.-C. Lau, Y. Xu, B. Xiong, Y.-C. Chang and C. Y. Ng, *J. Chem. Phys.*, 2014, **140**, 011102.

Table 1. ZPE corrected energies (in kcal mol^{-1}) of the stationary points at various levels.

	$H_2 + NH_2^-$	$NH_2^- \cdots H_2$	$NH_3 \cdots H^-$	$NH_3 + H^-$	NH_4^-	TS1	TS2	TS3
PIP-NN PES[a]	0	-2.11	-9.84	-2.17	7.78	0.02	-8.49	19.25
Ab initio[b]	0	-2.11	-9.84	-2.18	7.86	0.02	-8.55	19.32
Ab initio[c]	0	-2.11	-9.84	-2.18	7.86	0.02	-8.50	19.19
Ab initio[d]	0	-2.32	-10.25	-2.62	10.31	-0.43	-8.92	21.83
FI-NN PES[e]	0	-2.32	-10.40	-2.76		-0.56	-9.11	
Gianturco[f]	0	-2.33	-10.54	-2.97		-0.58		
Gianturco[g]	0	-4.43	-12.91	-3.85		-3.99		
Otto[h]	0	-2.31	-9.45	-3.23		-1.15		
Bohme[i]	0			-5.98				
ATcT[j]	0			-2.42				

[a] PIP-NN PES, this work;

[b] UCCSD(T)/AVTZ′, this work;

[c] CCSD(T)/AVTZ′, this work;

[d] CCSD(T)-F12a/AVTZ, this work;

[e] FI-NN PES;[11]

[f] CCSD(T)/AVTZ//MP2/AVTZ;[4]

[g] B3LYP/6-311++G**;[4]

[h] MP4/6-311++G**//MP2/6-31G;[1]

[i] Expt.;[7]

[j] ATcT.[6]

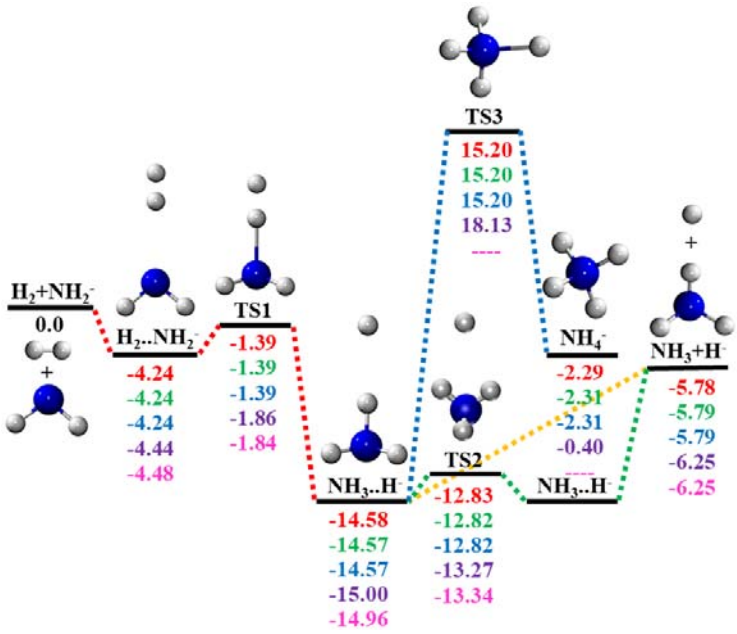

Fig. 1 Schematic illustration of the energetics along the reaction $H_2 + NH_2^-$. All energies are in kcal mol^{-1} and relative to the $H_2 + NH_2^-$ asymptote at various levels: PIP-NN PES, UCCSD(T)/AVTZ′, CCSD(T)/AVTZ′, CCSD(T)-F12a/AVTZ, FI-NN PES[11] from top to bottom.

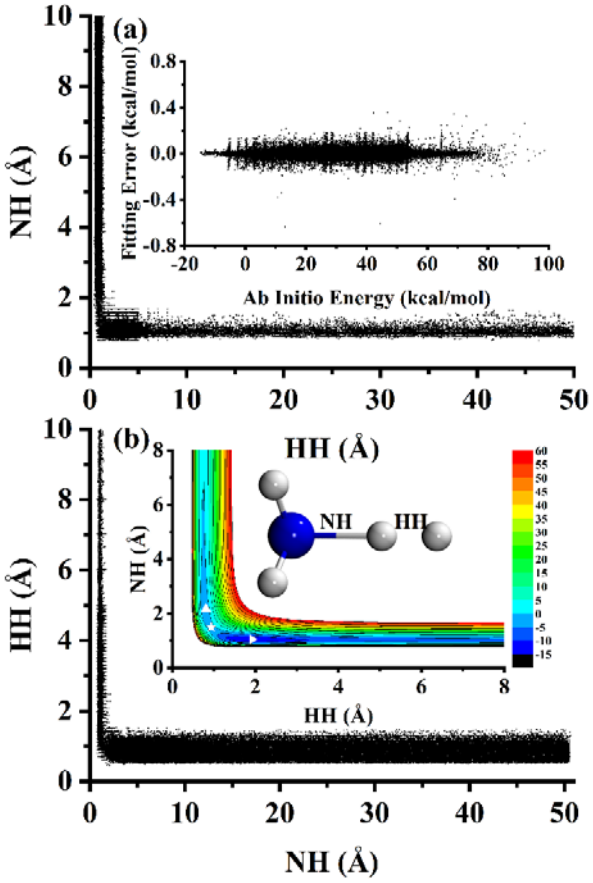

Fig. 2 (a)/(b) Distribution of the sampled points on the PIP-NN PES with the two reactive bond lengths up to 50 Å. The inset of **(a)** shows fitting errors ($E_{fit} - E_{target}$, in kcal mol^{-1}) for the PIP-NN PES as a function of the ab initio energy up to 100.0 kcal mol^{-1}. The inset of **(b)** displays the contour plot of the potential energies (in kcal mol^{-1}) for the process between $H_2 + NH_2^-$ and $NH_3 + H^-$ as a function of two reactive bond lengths, whose definitions are also shown. All other coordinates are fixed at TS1.

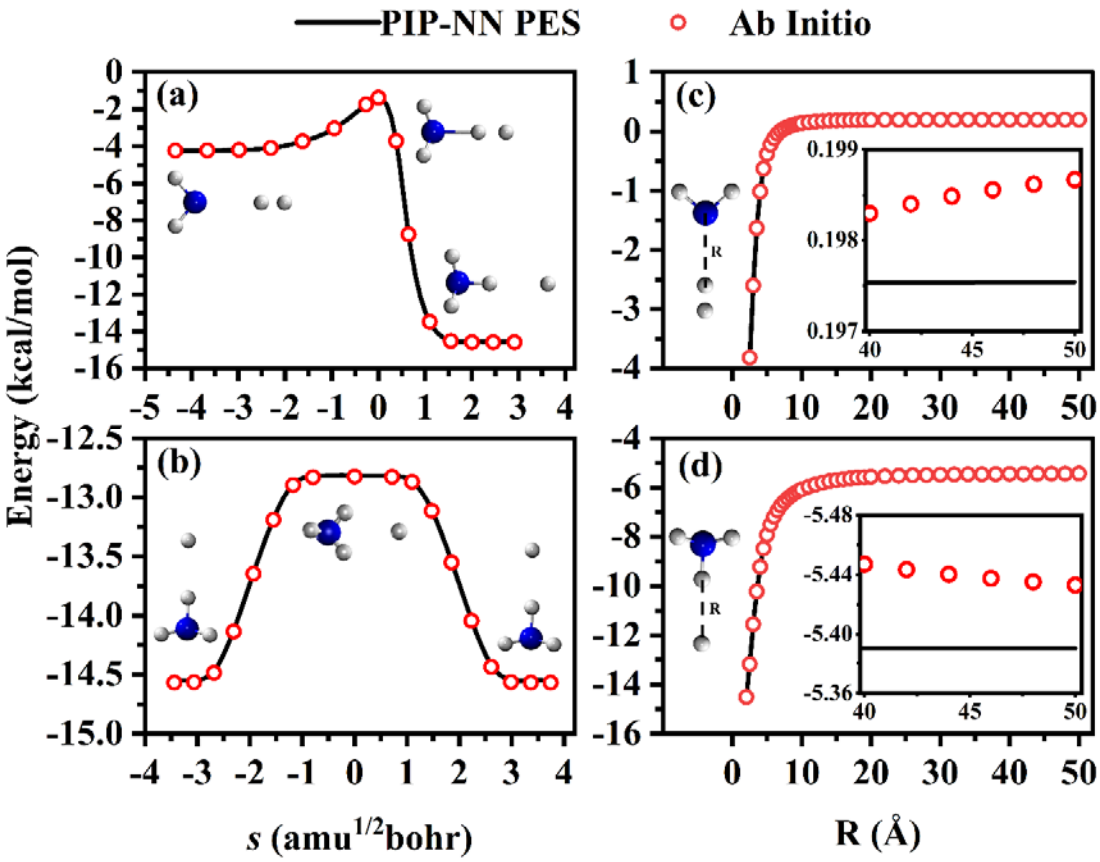

Fig. 3 Potential energies along the MEPs for the transformations between (**a**) $NH_2^-\cdots H_2$ and $NH_3\cdots H^-$, and (**b**) $NH_3\cdots H^-$ and $NH_3\cdots H^-$, as a function of the reaction coordinate *s* ($amu^{1/2}bohr$). One-dimensional cuts for the potential energy between NH_2^- and H_2 (**c**) and between NH_3 and H^- (**d**) along the *R* distance. The symbols represent the ab initio energies calculated at the UCCSD(T)/AVTZ′ level.

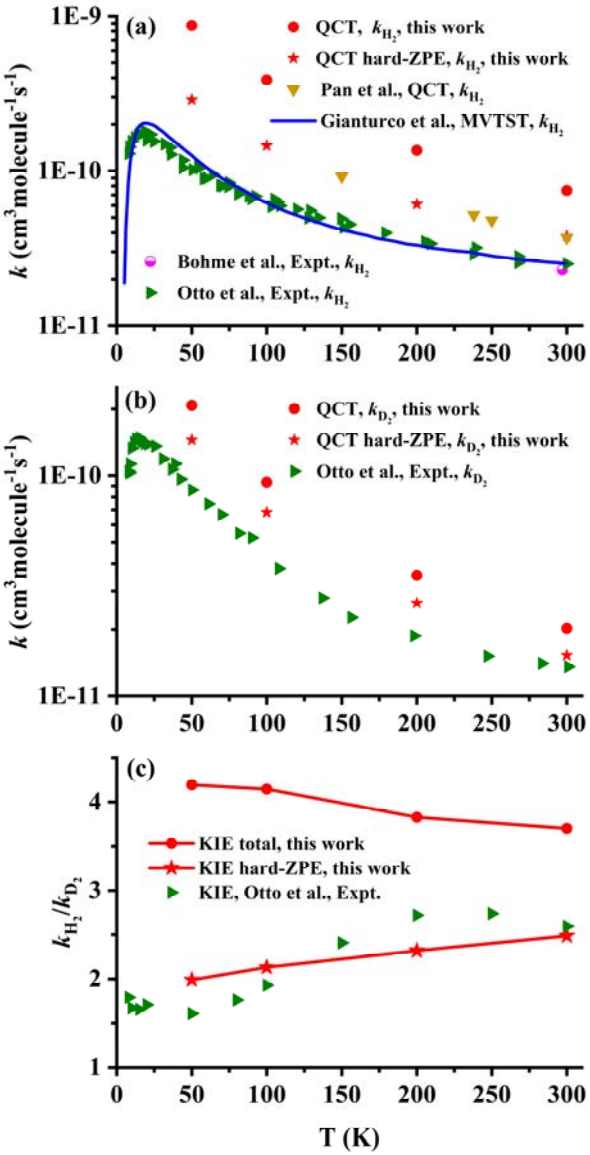

Fig. 4 Theoretical and experimental thermal rate coefficients for the $H_2 + NH_2^- \rightarrow NH_3 + H^-$ reaction (**a**) and the $D_2 + NH_2^- \rightarrow NH_2D + D^-$ reaction (**b**). The KIEs are plotted in (**c**). Available results from refs 1, 4, 7, 11 were included for comparison.

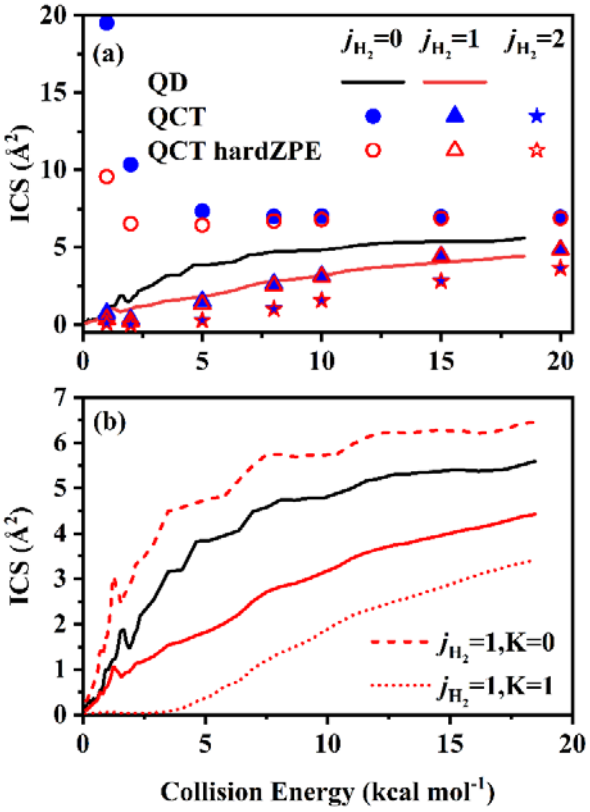

Fig. 5 (**a**) Integral cross sections (ICSs) for the reaction NH_2^- + H_2 (j=0, 1, 2) → NH_3 + H^- on the new PIP-NN PES as a function of the collision energy (in kcal mol^{-1}). (b) K-specific ICSs calculated by QD.

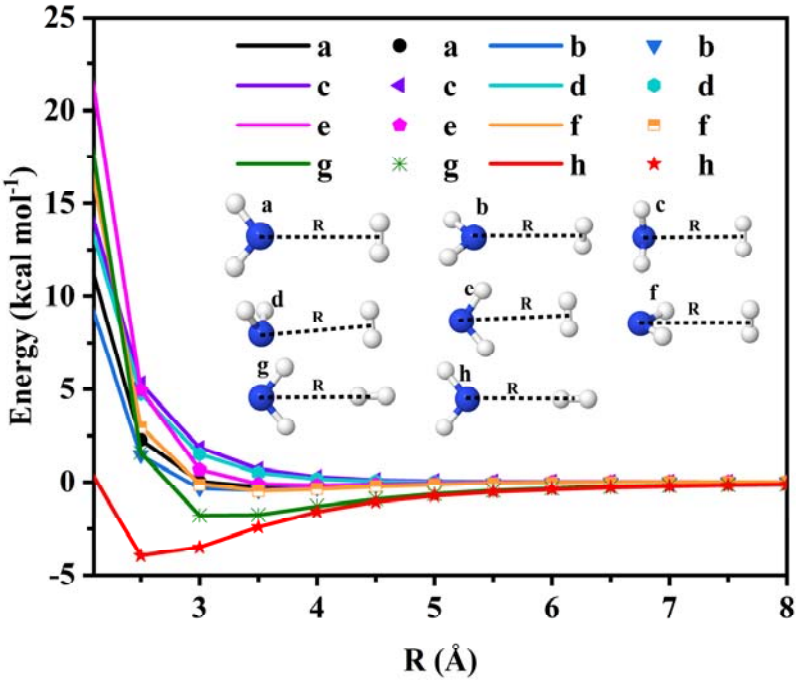

Fig. 6 Asymptotic potential energy curves between NH_2^- and H_2 at different orientations. Both NH_2^- and H_2 are fixed at equilibrium. The lines represent PIP-NN PES and symbols for *ab initio* energies.

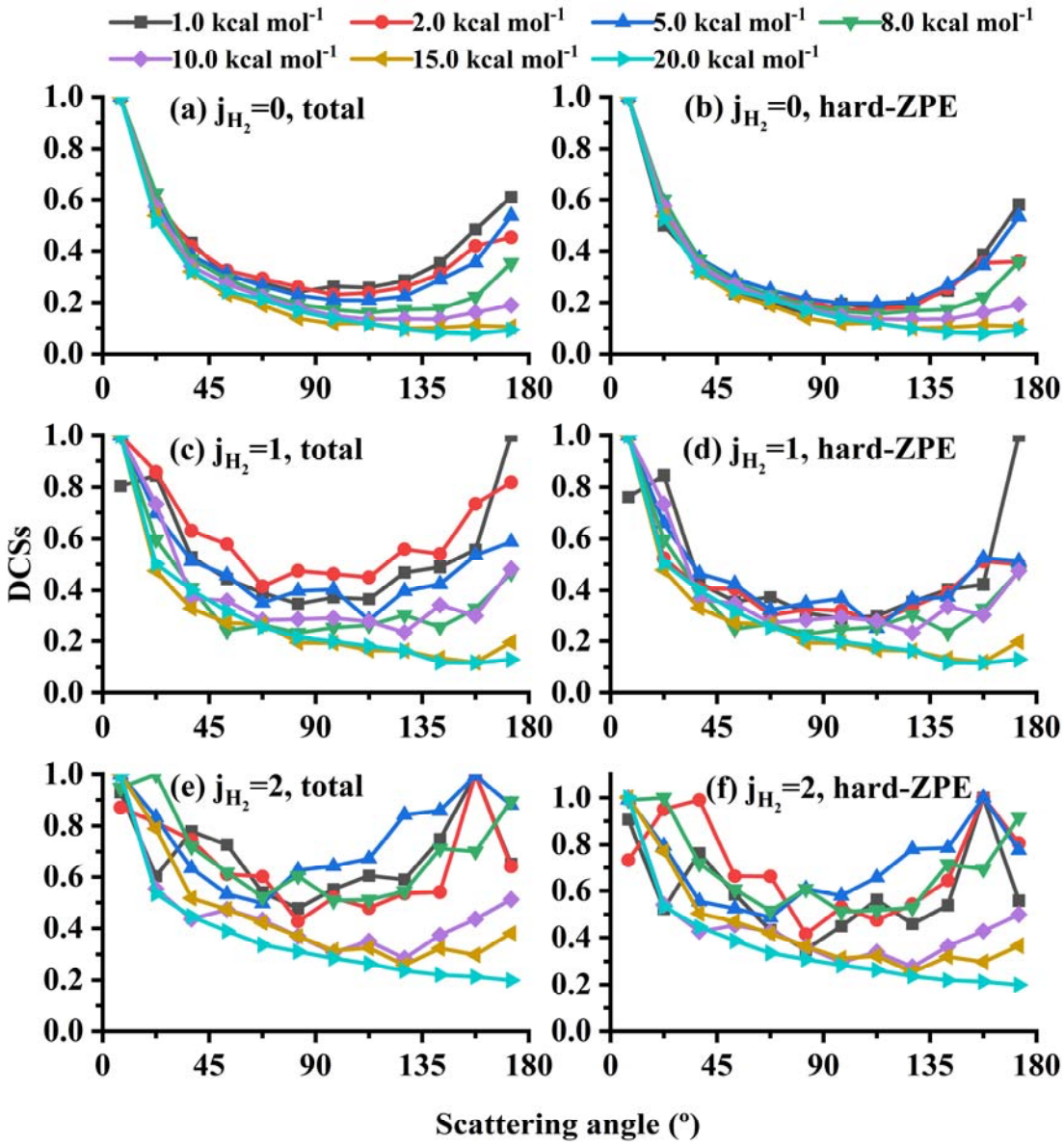

Fig. 7 Differential cross sections (DCSs) for the NH_2^- + H_2 (j=0, 1, 2) → NH_3 + H^- reaction at E_c = 1.0, 2.0, 5.0, 8.0, 10.0, 15.0, 20.0 kcal mol^{-1}.

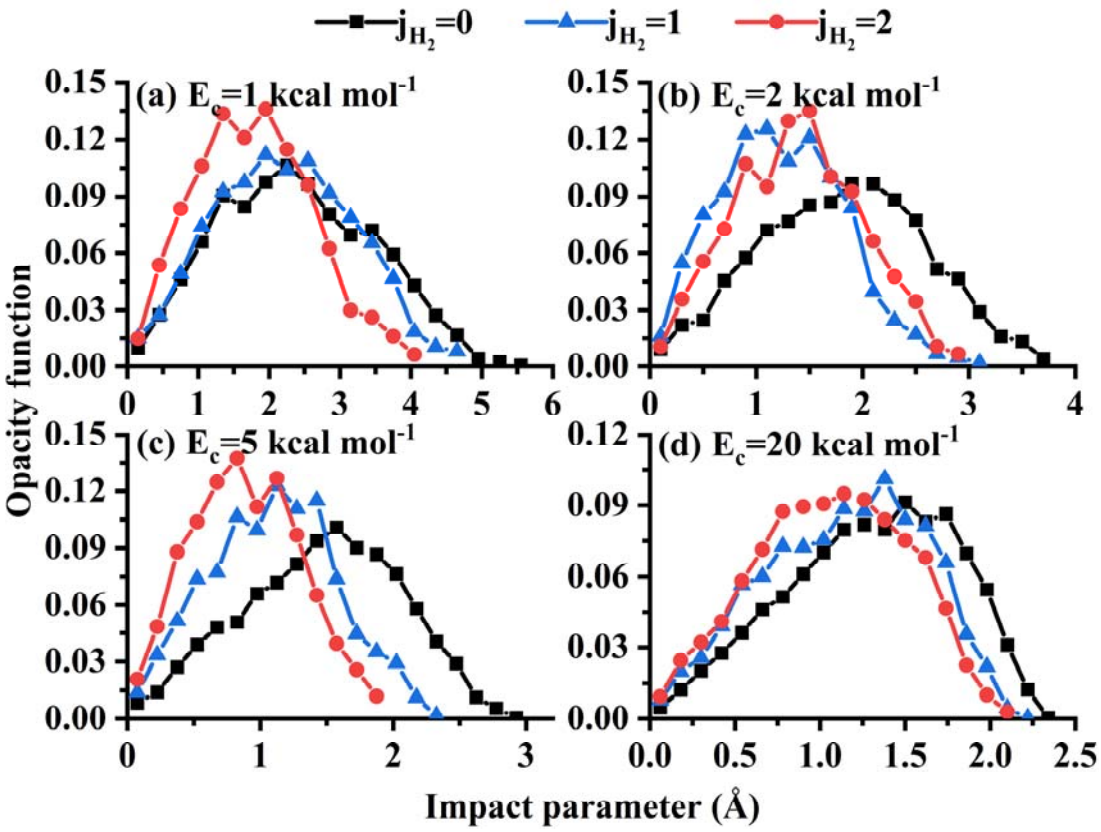

Fig. 8 Distributions of the impact parameters for the NH_2^- + H_2 (j=0, 1, 2) → NH_3 + H^- reaction at 1, 2, 5, 20 kcal mol^{-1}, respectively.

Table of content graphic

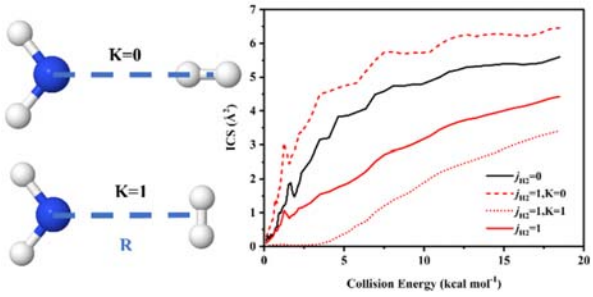

Both QCT and QD calculations on a full-dimensional accurate potential energy surface reveal a novel suppression of reactivity by exciting its reactant rotational mode.